Liquid-Liquid Flow Patterns in Reduced Dimension Based on Energy Minimization Approach

Aadithya Kannan, Subhabrata Ray, and Gargi Das
Dept. of Chemical Engineering, Indian Institute of Technology Kharagpur, Kharagpur 721302, West Bengal, India

DOI 10.1002/aic.15024
Published online September 10, 2015 in Wiley Online Library (wileyonlinelibrary.com)

Study of liquid-liquid flow patterns in reduced dimensions is relevant under the current trends to miniaturize process equipment. The phase distribution results from interplay of surface (dominant in microchannels) and gravity forces (dominant in larger dimensions). The proposed analysis, based on minimization of total system energy comprising of kinetic, surface, and potential energy, unravels the influence of wetting properties and predicts the range of existence of annular and plug flow as well as the onset of stratification with increasing conduit dimension. Unlike existing models marking abrupt transitions, the proposed methodology can predict zones of transition where interfacial distributions gradually evolve with change of operating conditions—the predictions agreeing closely to experimental and literature data. The analysis illustrates the coupled effect of diameter, contact angle, and inlet composition on flow distribution and defines the transition from macrodomain to microdomain (millichannels) in terms of Bond number as $0.1 < Bo < 10$.
 AIChE J, 62: 287–294, 2016
Keywords: energy minimization, plug flow, annular flow, mechanistic modeling, multiphase flow

Introduction

Two phase liquid-liquid flow is common in several practical applications like solvent extraction, reactive extraction, nitration, polymerization, and phase transfer catalysis. Miniaturization of process equipment has become important as it lowers mass- and heat-transfer resistances and leads to process intensification. Microcontactors with higher interfacial area leads to enhanced heat and mass transfer and microreactors achieve the advantage of fast intrinsic kinetics. This is because with miniaturization, the natural tendency of stratification due to gravity is offset by the increasing influence of surface forces and the plug flow pattern occurs over a wide range of operating conditions. In this pattern, capsular plugs of the nonwetting liquid traverse through the wetting liquid and present a periodic appearance of the flow phenomenon. This flow distribution although common in reduced dimensions, has scarcely been reported in large diameter pipes. A recent study[1] has revealed that plug flow in millimeter size channels favors mass transfer more than the other flow patterns. It is, therefore, relevant to know how the plug flow pattern metamorphoses to and from other flow patterns. This would help engineer small diameter devices and set the operating parameters to achieve the desired flow distribution.

Further, in small diameter conduits, the wetting properties of the liquids with respect to the wall become significantly important. It is often reported that the more wetting liquid forms a film at the conduit wall[2] while the other liquid flows through the central passage as droplets, plugs, or a continuous core depending on the relative proportions of the two. Interestingly, experiments by the present group have revealed that the liquid with a lower contact angle does not necessarily wet the conduit wall. For example, during toluene-water flow through 2 mm (0.002 m) and 6 mm (0.006 m) diameter glass conduits (glass-water contact angle, $\theta_1 = 32$–$34°$ and glass toluene contact angle, $\theta_2 = 5$–$6°$), it was expected that toluene would wet the tube wall in preference to water while experimental observations reveled that a pertinent water film always exists at the wall irrespective of the order of entry of the two liquids and their flow velocity. On the contrary, the same experiments performed in glass tubes coated with silane ($\theta_1 = 115$–$118°$, $\theta_2 = 16$–$18°$) have revealed toluene film at the wall under similar flow conditions.

While all these are interesting from a conceptual point of view, they raise difficulties whenever one desires to engineer a particular type of flow pattern, the concern being to determine a proper range of conditions within which such a pattern would prevail. A reasonable amount of literature[1–12] is available on flow patterns during liquid-liquid flow in narrow channels but no generic criterion to determine the range of existence of the different patterns has yet been suggested even for a simple circular geometry.

The present work attempts to predict the interfacial configurations of low viscous immiscible liquid flow in small diameter conduits from the principle of minimization of total system energy. There have been limited attempts to model multiphase flow from energy minimization considerations.[13–19] None of these analyses are applicable to reduced dimensions, where, in addition to gravity and kinetic energy, the surface energy component plays an important role in deciding the prevalent flow pattern. The focus on low to moderate flow rates of low viscous organic and aqueous phases is purposefully chosen to

Correspondence concerning this article should be addressed to A. Kannan at aadikan93@gmail.com.

avoid dominance of the kinetic energy component. We also define the domain of millichannels between the macroworld and the microworld. The flow distributions in millichannels display a unique physics of their own where both gravity and surface forces significantly contribute to the nature of flow.

Analysis

In the proposed analysis, expressions for steady-state total energy (per unit volume) content of the conduit system having specified geometry and orientation are developed for different flow patterns. The analysis of liquid-liquid flow is based on the principle that under steady-state conditions, the total energy holdup of the system is minimum for the stable flow pattern. A change in the input conditions (say phase flow rate) may disturb the balance between the energy components leading to a different flow pattern that exhibits the minimum energy under the changed condition. As mentioned earlier, for low to moderate flow rates of low viscous organic and aqueous phases, the total energy is postulated to comprise of kinetic energy (KE) and potential energy (PE) of the liquids as well as surface energy (SE) at the liquid-liquid and the solid-liquid interfaces. The postulation is valid for surface energy prevailing situations, where instabilities due to turbulent stresses and Kelvin Helmholtz type instabilities are negligible compared with surface energy-induced instabilities. Further, the hydrodynamic interfacial processes governed by Taylor instability do not apply to conduit dimensions equal to or less than the Laplace length scale.[20] Under these conditions, the nonwetting liquid flows either as a continuous tube (annular flow) or as cylindrical plugs (plug flow) through an annular film of the wetting liquid[1] and with increase in conduit diameter, stratification results in both the liquids wetting different proportions of the pipe wall.[21] Accordingly, the analysis is formulated for plug, annular, and stratified flow. Dispersed flow has not been modeled as the surface energy does not contribute significantly to total energy at high flow rates and the situation is kinetic energy dominant.

Flow of the aqueous and organic phase (designated as Liquid 1 and Liquid 2, respectively) is considered through a horizontal conduit of finite length (L) and diameter (d). Although the analysis can be extended to conduits inclined to the horizontal, the horizontal orientation is chosen to identify stratification, if it appears as a stable option. The individual energy terms are considered with respect to corresponding reference values (KE_0, SE_0, PE_0), for flow of only the water phase at the mixture velocity ($u_1 + u_2$) through the conduit where u_1 and u_2 are the liquid superficial velocities obtained by dividing the inflow rates with conduit cross section ($\pi d^2/4$).

The expressions for the reference energy hold up in the conduit are

$$KE_0 = \frac{\pi d^2 L \rho_1 (u_2+u_1)^2}{8} \tag{1a}$$

$$SE_0 = \pi d L \sigma_{1s} \tag{1b}$$

$$PE_0 = \frac{\pi d^3 L \rho_1 g}{8} \tag{1c}$$

where ρ_1 is the density of liquid 1, σ_1 is the surface tension of Liquid 1, and g is the acceleration due to gravity. This gives the nondimensional energy terms for a particular flow pattern as

$$\Delta PE_{pattern} = \frac{PE_{pattern} - PE_0}{KE_0} \tag{2a}$$

$$\Delta KE_{pattern} = \frac{KE_{pattern} - KE_0}{KE_0} \tag{2b}$$

$$\Delta SE_{pattern} = \frac{SE_{pattern} - SE_0}{KE_0} \tag{2c}$$

The nondimensional total energy is therefore

$$\Delta TE_{pattern} = \Delta PE_{pattern} + \Delta KE_{pattern} + \Delta SE_{pattern} \tag{3}$$

The geometric parameters defining the flow configuration and those required for developing the energy expression for each flow pattern is shown in Figure 1. Expressions for steady-state total energy (per unit volume) content of the conduit system for different flow patterns are developed by assuming idealized (fully developed steady state) flow with a smooth liquid-liquid interface. In addition, each flow pattern specific model is based on certain assumptions inferred from the experimental observations of the flow patterns. Slip between the phases, if any, is taken care of, by allowing the *in situ* volume fraction of Liquid 2 (α) to be different from the corresponding inlet volume fraction β expressed as $\beta = u_2/(u_1+u_2)$.

Energy expressions for annular flow (Figure 1a) is formulated for concentric as well as eccentric core by assuming negligible energy dissipation due to wall friction (valid for low viscous liquids) and no wall liquid entrained in the core (Liquid 2). This is in agreement with the visual observations of annular flow in confined environment[1] and gives the individual energy terms for a concentric core as

$$\Delta PE_A = \frac{g\alpha d}{(u_2+u_1)^2}\left(\frac{\rho_2}{\rho_1} - 1\right) \tag{4}$$

$$\Delta KE_A = \frac{\rho_2 \beta^2}{\rho_1 \alpha} + \frac{(1-\beta)^2}{1-\alpha} - 1 \tag{5}$$

$$\Delta SE_A = \frac{8\sigma_{12}}{d\rho_1 (u_2+u_1)^2}\sqrt{\alpha} \tag{6}$$

In the above expressions, ρ_1 and ρ_2 are the respective densities of Liquids 1 and 2. σ_{12}, σ_1 and σ_2 denote interfacial tension of the liquid pair and the surface tension of Liquids 1 and 2 on the solid surface in presence of air, and α and β refer to the *in situ* and inlet volume fraction of Liquid 2.

The eccentric core annular flow (Figure 1b) model differs only in the potential energy term. The top surface of the eccentric core is assumed to be at infinitesimal distance from the conduit surface. This gives the potential energy (ΔPE_{EA}) for eccentric core annular flow as

$$\Delta PE_{EA} = \frac{g\alpha d}{(u_2+u_1)^2}\left(\frac{\rho_2}{\rho_1} - 1\right)(2-\sqrt{\alpha}) \tag{7}$$

The eccentric core annular flow pattern evolves into stratified flow as gravity overrides in larger conduits. Considering the pronounced wall effect in small channel dimensions, the energy components in stratified flow (Figure 1c) have been modeled for a curved (circular arc) liquid-liquid interface following the methodology proposed by Brauner et al.[14]

This gives

$$\Delta PE_S = \frac{(1-\alpha) g \rho_1 h_1 + \alpha g \rho_2 h_2}{\frac{\rho_1 (u_2+u_1)^2}{2}} - \frac{dg}{(u_2+u_1)^2} \tag{8}$$

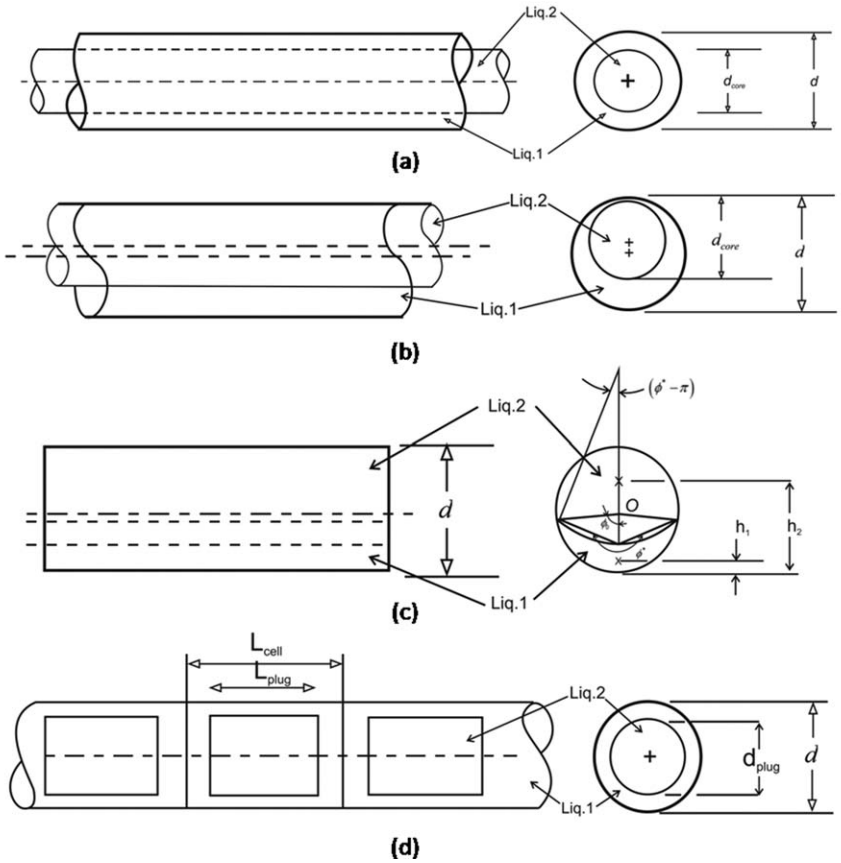

Figure 1. Geometrical representation of (a) annular flow, (b) eccentric annular flow, (c) stratified flow, and (d) plug flow.

$$\Delta \mathrm{KE_S} = \frac{\rho_2 \beta^2}{\rho_1 \alpha} + \frac{(1-\beta)^2}{1-\alpha} - 1 \tag{9}$$

$$\Delta \mathrm{SE_S} = \frac{(\pi - \phi_o)\sigma_2 + \phi_o \sigma_1 + \sigma_{12}(\pi - \phi^*)(\sin(\phi_o)/\sin(\phi^*)) - \sigma_1}{\frac{d\rho_1 (u_2+u_1)^2}{8}} \tag{10}$$

h_1 and h_2 are the height of the center of gravity of the channel cross section occupied by Phases 1 and 2, respectively, measured from the bottom of the conduit (Figure 1c). In a conduit of diameter "d," the cross-section geometry is defined by the independent parameters, ϕ_o and ϕ^*. These fix the other variables, α, h_1, and h_2 appearing in the expressions. Explicit algebraic expressions derived from geometry are elaborated by Brauner et al.[14]

The plug flow (Figure 1d) analysis considers several unit cells of equal length (L_{cell}) where each cell comprises of a plug of each liquid. Axisymmetric cylindrical plugs have been observed and have also been suggested.[22] The potential energy term is, therefore, based on axisymmetric liquid plugs. The energy terms in this case are

$$\Delta \mathrm{PE_P} = \frac{g \alpha d}{(u_2+u_1)^2} \times \left(\frac{\rho_2}{\rho_1} - 1\right) \tag{11}$$

$$\Delta \mathrm{KE_P} = \frac{\rho_2 \beta^2}{\rho_1 \alpha} + \frac{(1-\beta)^2}{1-\alpha} - 1 \tag{12}$$

$$\Delta \mathrm{SE_P} = \frac{4\sigma_{12}}{d^2 \rho_1 (u_2+u_1)^2 \mathrm{L_{cell}}} \times (d_{\mathrm{plug}}^2 + 2 d_{\mathrm{plug}} L_{\mathrm{plug}}) \tag{13}$$

Equation 13 requires additional information regarding the diameter (d_{plug}) and length (L_{plug}) of the plugs of Liquid 2. An empirical correlation with $R^2 = 0.906$ has been developed for the stable plug length (L_{plug}/d) from experimental data[23] during toluene-water flow in 2 mm (0.002 m) and 6 mm (0.006 m) diameter conduits

$$\frac{L_{\mathrm{plug}}}{d} = (1.3 + 15u_2 + 6u_1)(1000d)^{0.44} \tag{14}$$

The above expression of plug length (L_{plug}, m) as a function of phase superficial velocities (u_1, u_2, m/s) and conduit diameter (d, m) has further been validated with the experimental data reported by Jovanovic et al.[8] for toluene-water flow in 248 μm (2.48×10^{-4} m) and 498 μm (4.98×10^{-4} m) diameter microchannels—the extent of mismatch lying within 10–15% for the provided data.

The nondimensional expressions for total energy are algebraically transformed in terms of relevant nondimensional numbers

$$\Delta \mathrm{TE_A} = \frac{1}{Fr_{\mathrm{m}}}\left(\frac{\rho_2}{\rho_1} - 1\right)\alpha + \frac{\rho_2 \beta^2}{\rho_1 \alpha} + \frac{(1-\beta)^2}{1-\alpha} - 1 + \frac{8\sqrt{\alpha}}{We_{\mathrm{m}}}\left\{1 - \alpha\left(1 - \frac{\rho_2}{\rho_1}\right)\right\} \tag{15}$$

$$\Delta \mathrm{TE_{EA}} = \frac{1}{Fr_{\mathrm{m}}}\left(\frac{\rho_2}{\rho_1} - 1\right)\alpha(2 - \sqrt{\alpha}) + \frac{\rho_2 \beta^2}{\rho_1 \alpha} + \frac{(1-\beta)^2}{1-\alpha} - 1 + \frac{8\sqrt{\alpha}}{We_{\mathrm{m}}}\left\{1 - \alpha\left(1 - \frac{\rho_2}{\rho_1}\right)\right\} \tag{16}$$

$$\Delta TE_S = \left(\frac{2(1-\alpha)h_1}{d}\right)\frac{1}{Fr_m} + \left(\frac{2\alpha h_2}{d}\right)\frac{1}{Fr_m}\frac{\rho_2}{\rho_1} - \frac{1}{Fr_m} + \frac{\rho_2\beta^2}{\rho_1\alpha} + \frac{(1-\beta)^2}{1-\alpha} - 1 + \frac{8(\pi-\phi_o)}{Bo_1 Fr_m}\frac{\rho_2}{\rho_1} + \frac{8\phi_o}{Bo_2 Fr_m} + \frac{8}{We_m}\left(1-\frac{\rho_2}{\rho_1}\right)\frac{(\pi-\phi^*)}{\pi}\frac{\sin(\phi_o)}{\sin(\phi^*)} - \frac{8}{We_m} \quad (17)$$

$$\Delta TE_P = \frac{1}{Fr_m}\left(\frac{\rho_2}{\rho_1}-1\right)\alpha + \frac{\rho_2\beta^2}{\rho_1\alpha} + \frac{(1-\beta)^2}{1-\alpha} - 1 + \frac{4}{We_m}\left(\frac{\alpha d}{L_{plug}} + \frac{\alpha d}{d_{plug}}\right) \quad (18)$$

The above expressions reveal that the same nondimensional groups appear in each of the equations–Froude number $\left(Fr_m = \frac{(u_2+u_1)^2}{gd}\right)$ and Weber number $\left(We_m = \frac{(u_2+u_1)^2}{\sigma_{12}}(\rho_1 - \rho_2)\, d = Fr_m Bo_m\right)$ for the liquid-liquid mixture which quantify the importance of inertia over gravity and capillary force, respectively. Other nondimensional ratios are inlet (β) and *in situ* (α) volume fractions of Liquid 2 and the liquid density ratio $\left(\frac{\rho_2}{\rho_1}\right)$. The additional appearance of Bond number of the individual liquids $\left(Bo_2 = \frac{\rho_2 g d^2}{\sigma_2}$ and $Bo_1 = \frac{\rho_1 g d^2}{\sigma_1}\right)$ in stratified flow model is natural, considering the antagonist roles of buoyancy and interfacial forces when both the liquids contact the pipe wall.

To understand the wall wetting characteristics in reduced dimensions, the total energy expressions for annular and plug flow with Liquid 2 wetting the conduit wall are also considered. Considering the terminology (dispersed and inverted dispersed) adopted in literature[1,21,24,25] to distinguish between oil in water and water in oil flow patterns, these patterns are termed inverted annular flow and inverted plug flow. Total energy expressions in terms of the relevant nondimensional parameters for these two cases are

$$\Delta TE_{IAConcentric} = \frac{1}{Fr_m}\left(\frac{\rho_2}{\rho_1}-1\right)\alpha + \frac{\rho_2\beta^2}{\rho_1\alpha} + \frac{(1-\beta)^2}{1-\alpha} - 1 + \frac{8\sqrt{\alpha}}{We_m}\left\{\left(\frac{\sigma_1\cos(\theta_1)-\sigma_2\cos(\theta_2)}{\sigma_{12}}\right) + \sqrt{1-\alpha}\right)\right\} \quad (19)$$

$$\Delta TE_{IP} = \frac{1}{Fr_m}\left(\frac{\rho_2}{\rho_1}-1\right)\alpha + \frac{\rho_2\beta^2}{\rho_1\alpha} + \frac{(1-\beta)^2}{1-\alpha} - 1 + \frac{4}{We_m}\left(\frac{\alpha d}{L_{plug}} + \frac{\alpha d}{d_{plug}}\right) + 8\left(\frac{\sigma_1\cos(\theta_1)-\sigma_2\cos(\theta_2)}{\sigma_{12}}\right) \quad (20)$$

Model Solution

In each expression for total energy, the input variables are d, u_1, u_2, ρ_1, ρ_2, σ_{12}, σ_1, and σ_2. The rest of the variables are parameters that define the geometry of the flow morphology. Given a set of numerical values of the input data, the expression for steady-state total energy for each pattern can be parametrically minimized to obtain the minimum energy states corresponding to each flow pattern. This optimization (minimization) procedure is carried out using the routine LSQNONLIN with modified Levenberg–Marquardt algorithm option in MATLAB® software (Ver.7, M/s Mathworks).

The globally minimum energy suggests the stable pattern for the set of input variables. However, in case of plug flow, an additional constraint on stable plug length range is required to be satisfied. This constraint, associated with instability, is expected to have limits that would have a stochastic level of uncertainty. Limits of this constraint, $10 < (L_{plug}/d) < 20$, are therefore statistically derived from experimental data reported in literature.[23] Satisfying both the criteria of minimum total energy and plug length ensures stable plug flow. If either of the conditions is not satisfied, the pattern is evolving from segregated to plug flow or vice versa. We further envisage that a close value of minimum total energy (ΔTE_{min}) for any two patterns suggests that the flow under this condition can exhibit characteristics of both and consequently lies in the transition zone. A check for the closeness of total (minimum) energy for plug flow and annular flow is, therefore, incorporated with the limit of closeness set to 7.5% where the limit is defined as $\left|100X\frac{\Delta TE_A - \Delta TE_P}{0.5(\Delta TE_A + \Delta TE_P)}\right| = 7.5$. This percentage is chosen based on the experimental identification of the zones of transition between flow regimes. The accuracy of the prediction is later elucidated in Figure 3. Incorporation of this check leads to plug-annular and plug-stratified transition options being arrived at. This consideration enables the proposed analysis to predict both the range of existence of the different patterns as well as the zones of transition where interfacial distributions gradually evolve into a different set with change of operating conditions. The conditions and constraints leading to the different flow patterns are summarized in Table 1.

Table 1. Conditions for Existence of Different Flow Patterns

Flow Pattern	Condition for Existence
Stratified	$\Delta TE_S = \min(\Delta TE_A, \Delta TE_S, \Delta TE_P)$
Annular	$\Delta TE_A = \min(\Delta TE_A, \Delta TE_S, \Delta TE_P)$ (Lplug/d) >20; Deviation between ΔTE_P and ΔTE_A <7.5%
Plug	$\Delta TE_P = \min(\Delta TE_A, \Delta TE_S, \Delta TE_P)$ (Lplug /d) < 10
Plug-annular transition	$\Delta TE_P = \min(\Delta TE_A, \Delta TE_S, \Delta TE_P)$ 10< (Lplug/d) <20; $\Delta TE_A < \Delta TE_S$
Plug-stratified transition	$\Delta TE_P = \min(\Delta TE_A, \Delta TE_S, \Delta TE_P)$ 10< (Lplug/d) <20; $\Delta TE_S < \Delta TE_A$

Repeating this procedure identifies the most stable flow pattern corresponding to different input datasets and a flow pattern map (Figure 3) is drawn that includes the zones of flow pattern transitions. It may be noted that in reality, pattern transitions are gradual although the theoretical models even in large diameter tubes[24] have predicted discrete curves marking an abrupt transition between subsequent patterns. The entire procedure for arriving at the stable flow pattern including the transition zones is presented in Figure 2, in the form of a flow chart.

Model Validation

The flow pattern maps obtained from theoretical analysis are validated with toluene-water experimental data in 2 mm (0.002 m) and 6 mm (0.006 m) diameter conduits.[1] Both glass and silanized glass conduits have been used for these experiments. In the test rigs, two diametrically opposite channels collect the liquids into a main stream, the system forming a T-type injection configuration. The combined flow occurs through the horizontal conduit of length 1 m in the 2 mm conduit and 1.5 m in the 6 mm (0.006 m) conduit. Images captured at 500 frames per second over a length of 10 cm (0.1 m) of the conduit are analyzed to identify the prevailing flow pattern. To ensure fully developed flow, the visualization section

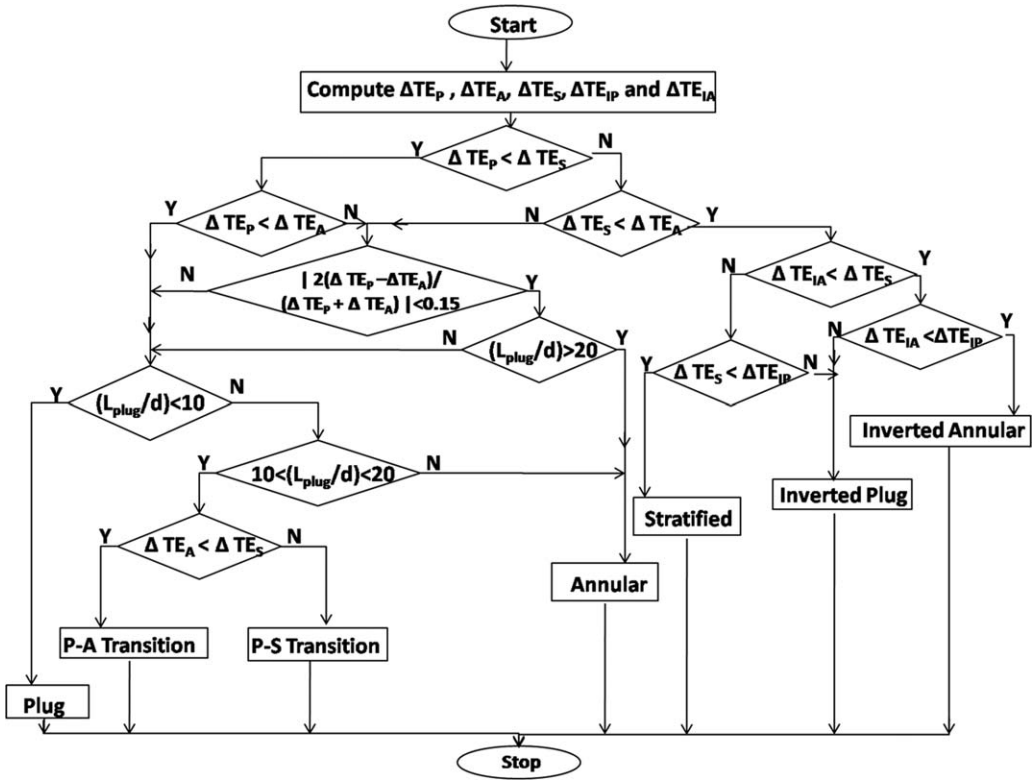

Figure 2. Algorithm to identify the stable flow pattern based on energy minimization approach.

is located beyond 300 mm (0.3 m) in the 2 mm (0.002 m) capillary and 700 mm (0.7 m) in the 6 mm (0.006 m) tube. The details on experimentation are reported elsewhere.[1]

The inset of Figure 3 where the superficial velocity of water (Liquid 1) is plotted against the superficial velocity of toluene (Liquid 2) represents a typical flow pattern map. It displays all the flow patterns observed for flow rates up to 3.14×10^{-6} m^3/s in the 2 mm (0.002 m) diameter glass conduit. Isolated cylindrical structures flowing with the mean flow velocity are obtained at low toluene and water flow rates. Once the plugs are formed, they are entrained by the flow and their shape does not evolve any further. As the toluene volume fraction increases, the interfacial instability leading to the "pinching effect" ceases to hold presumably because inertial forces (which increase with flow rate) now prevail over capillarity. As a consequence, a continuous toluene core flows through an annular water film and gives rise to the annular flow regime. Dispersed flows occur at higher water and toluene flow rates corresponding to the upper left and lower right portions of the figure. The nature of flow was noted to change drastically in silanized glass tubes ($\theta_1 = 120°$, $\theta_2 = 18°$) with water flowing as plugs and a continuous tube through an annular toluene film.

The experimental conditions are simulated with the proposed flow regime models in the zone of interest as highlighted in the inset of Figure 3a. These have been simulated with the liquid properties: $\rho_1 = 1000$ kg/m^3, $\rho_2 = 850$ kg/m^3; $\sigma_{12} = 36 \times 10^{-3}$ N/m; $\sigma_1 = 72 \times 10^{-3}$ N/m; $\sigma_2 = 28.5 \times 10^{-3}$ N/m; to understand the effect of diameter on flow pattern, the simulation exercise has also been repeated with property values for kerosene-water experimental data in a 12 mm (0.012 m).[21] The theoretical map with the experimental transition lines is depicted in Figure 3. The accuracy of prediction is evident from the figures. The percentage mismatch (quantified as the fraction (in %) of the total number of theoretically predicted data points which do not agree with the experimentally determined flow pattern) lies within 8–10% for the three test cases with the points of mismatch being close to the experimental boundaries demarcating the flow patterns.

To explore the robustness of the analysis, additional validations with data from literature has been attempted. Only a limited number of published studies providing all the inputs required by the model could be located. A comparison with toluene-water data reported by Kashid and Minsker[7] in a rectangular conduit shows correct prediction for more than 80% of the data points. They proposed a parameter $Re_2 d/\beta$ (m) related to plug-annular transition boundary, where Re_2 ($= \rho_2 u_2 d/\mu_2$) is the Reynolds number of Liquid 2. This shows that the transition parameter increases with conduit diameter. They have reported the transition to occur at $Re_2 d/\beta = 1.5$ m for a conduit diameter of 0.269 mm (2.69×10^{-4} m), The plug-annular transition predicted from our analysis and algorithm correspond to the $Re_2 d/\beta$ value of 4 m and 6 m for conduit diameters of 2 mm (0.002 m) and 6 mm (0.006 m), respectively. The trend based on extrapolation with respect to diameter is evident. Further, Tsaoulidis et al.[10] reported plug-annular transition to occur at $\beta = 0.3$ in a 200 μm microchannel while the same is predicted to occur at $\beta = 0.5$ by the present analysis. We do acknowledge that the completeness of physical properties and interfacial energies reported by them have contributed to the closeness of prediction (% mismatch $< 25\%$) in the latter case.

Discussions

A close observation of the energy expressions reveal that tube diameter is a key parameter for organizing the different

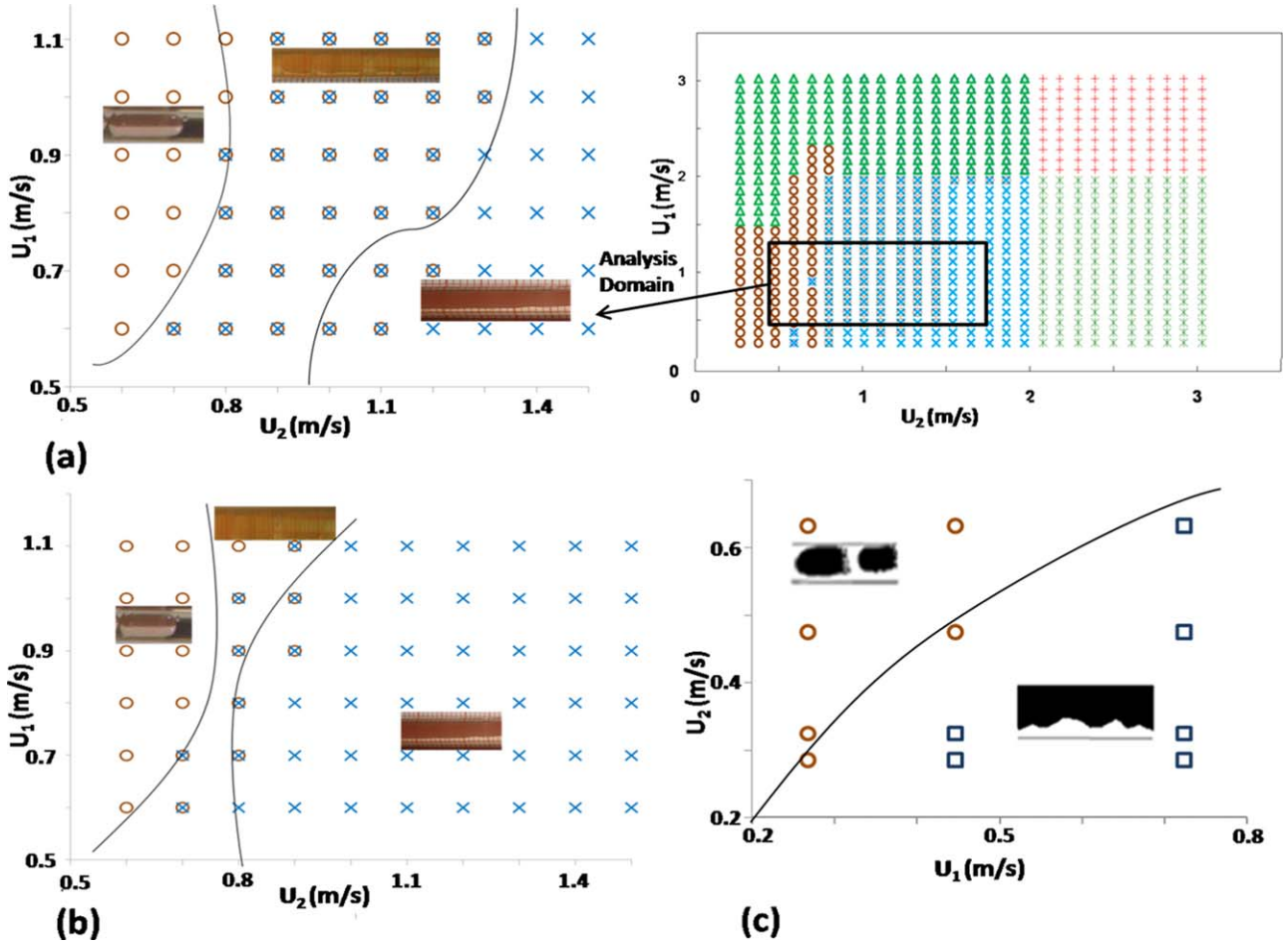

Figure 3. Model prediction vis-à-vis experimental flow pattern in analysis domain, toluene water flow in glass conduit of diameter (a) 0.002 m, (b) 0.006 m, and (c) 0.012 m for kerosene-water flow.

Legends denote model prediction (○, plug; ×, annular; ⊠, plug/annular transition; □, stratified) and curves denote experimental boundaries. Inset of (a) depicts the experimental phase diagram with the analysis domain marked in a 0.002 m conduit (△, dispersed; ✳, inverted dispersed). [Color figure can be viewed in the online issue, which is available at wileyonlinelibrary.com.]

effects into a hierarchy. Accordingly, a pictorial depiction of flow pattern behavior with diameter as obtained from the energy minimization analysis is presented in Figure 4. The figure depicts the flow patterns for a constant mixture velocity with toluene and water flowing in a glass conduit. It also includes the ΔTE_{min} comparison, highlighting the tradeoff between surface and potential energies. The model predictions are consistent with the experimental observations. The domain of plug flow expands with decrease of conduit diameter and inlet volume fraction of toluene. Conversely, an increase in diameter attempts to segregate the phases and ensures wall wetting by both the liquids—the inlet volume fraction (β) of toluene complementing the diameter effect. Thus, while plug formation is favored at low d and β, stratification is the natural tendency at the other extreme. However, at small proportions, the wetting liquid (toluene) prefers to adhere to the conduit wall.

The effect of d and β on the resulting stable flow pattern is presented in Figure 5 for toluene-water flow through hydrophobic and hydrophilic conduits. Figure 5a presents the minimum total energy for two inlet fractions (0.5 and 0.9) of toluene. The two curves for the different flow patterns have all input conditions same, except the conduit diameter. Results from the analysis for a typical hydrophobic conduit are presented in Figure 5b.

Interestingly, the annular and plug distributions compete to be energetically privileged for narrow conduits ($d < 0.01$ m) and the inlet phase composition governs the stable flow pattern. This is evidenced by Figure 5a where we find that beyond a threshold β (≈ 0.9), plug flow ceases to be stable as the low inlet water fraction fails to segregate the toluene plugs. The figure further reveals that in hydrophilic tubes, the tendency to stratify is pronounced for $d > 0.015$ m for all β. This corresponds to $Bo_{mix} \approx 10$. Nevertheless, the curves are very close for stratified and eccentric core at high β (≈ 0.9). This suggests stratified-annular transition and hints at the tendency of stratification with a continuous water film at $d > 0.015$ m. We note from the figure that for hydrophobic conduits, stratification is predicted only beyond a conduit diameter of $\sim$10 cm (0.1 m).

The aforementioned observations show that the wall wetting liquid for liquid-liquid flow is not decided by the individual contact angles alone but by the liquid-liquid contact angle θ_{12} defined through the relation

$$\cos(\theta_{12}) = \left(\frac{\sigma_1 \cos(\theta_1) - \sigma_2 \cos(\theta_2)}{\sigma_{12}} \right) \tag{21}$$

θ_{12} is a function of surface tension and contact angle of the individual liquids and a value of θ_{12} close to 90° ($\theta_1 \sim 65°$)

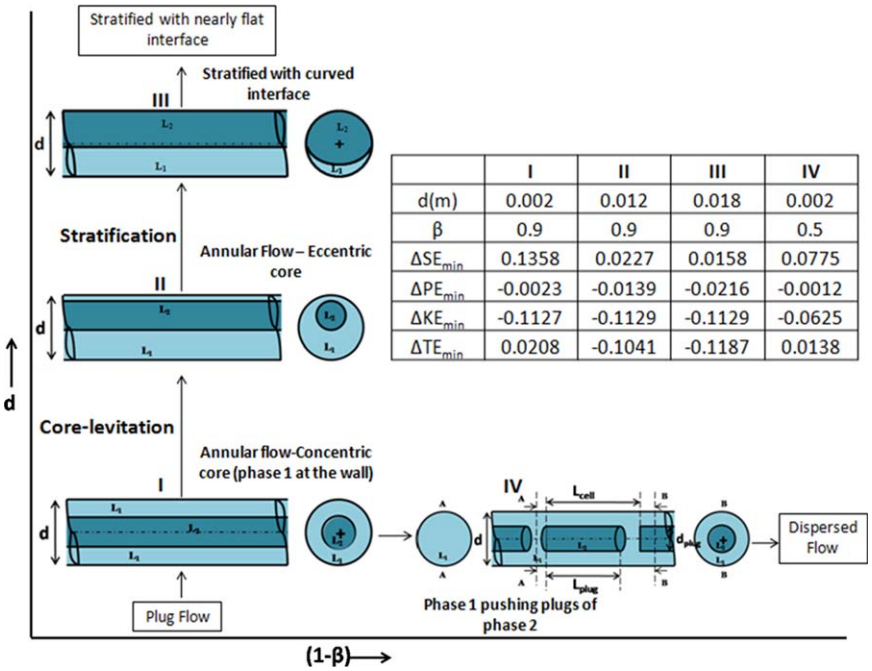

	I	II	III	IV
d(m)	0.002	0.012	0.018	0.002
β	0.9	0.9	0.9	0.5
ΔSE_{min}	0.1358	0.0227	0.0158	0.0775
ΔPE_{min}	-0.0023	-0.0139	-0.0216	-0.0012
ΔKE_{min}	-0.1127	-0.1129	-0.1129	-0.0625
ΔTE_{min}	0.0208	-0.1041	-0.1187	0.0138

Figure 4. Influence of d and β on flow pattern, a pictorial representation (u_m =1 m/s, $\theta_1 = 30^\circ$, $\theta_2 = 8^\circ$).

Inset table highlights the tradeoff between potential and surface energies. [Color figure can be viewed in the online issue, which is available at wileyonlinelibrary.com.]

marks the shift in the wall wetting liquid. The effect of contact angle is corroborated by the expression of the surface energy terms for the inverted annular and inverted plug flow patterns.

We propose to define the domain of millichannels based on the analysis by postulating that the lower limit is when the eccentric core and concentric core energies differ by less than 10% ($d = 0.002$ m) and the upper limit is with the surface energy component being approximately equal to the potential energy ($d = 0.015$ m). In two-phase flow, the Bond number value is often used to distinguish between macrosystem and microsystem.[20] On this basis, we express the aforementioned criteria in terms of mixture Bond number. The corresponding limits for the Bo_{mix} are: ~0.1 and ~10. It is worth noting that the different critical values of Bond number experimentally

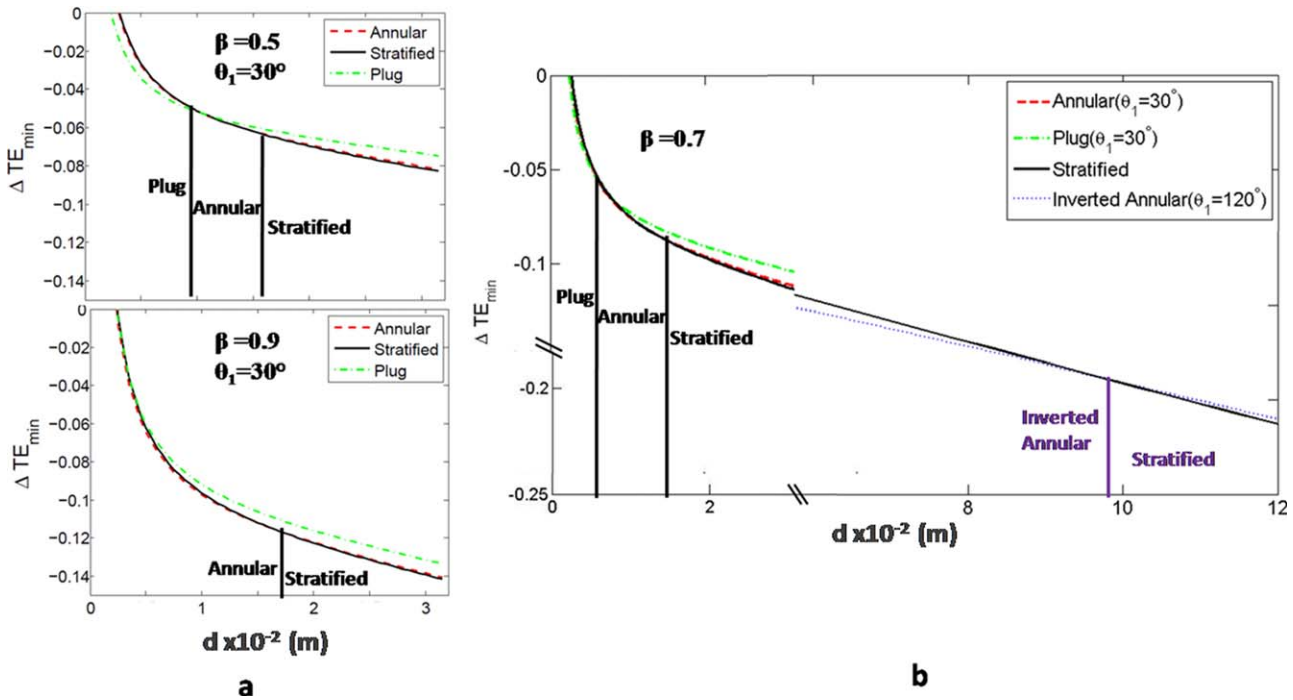

Figure 5. Effect of diameter on phase distribution at a constant mixture velocity ($u_m = 1$ m/s) for (a) $\beta = 0.5$ and 0.9 in a hydrophilic ($\theta_1 = 30^\circ$) conduit, (b) $\beta = 0.7$ and θ_1 as parameter: onset of stratification at $d = 0.016$ m for $\theta_1 = 30^\circ$, $\theta_2 = 8^\circ$ and at $d = 0.098$ m for $\theta_1 = 120^\circ$, $\theta_2 = 18^\circ$.

[Color figure can be viewed in the online issue, which is available at wileyonlinelibrary.com.]

arrived to mark the transition between small and large diameter tubes (Suo and Griffith[26]—0.22, Brauner et al.[14]—1.0) lie within the proposed limit. These experimental studies were on larger diameter tubes where the surface forces are less contributive. As the study attempts to predict flow patterns based on the fundamental principle of energy minimization, corroboration of the Bond number range for small diameter channels with literature data is an additional validation of the approach.

Conclusions

The energy minimization principle coupled with the theoretical model developed can be reliably used for predicting the flow patterns of low viscous liquid-liquid flow in reduced dimensions. It is applicable for both hydrophilic and hydrophobic conduits and has been validated for low to moderate flow rates where in addition to kinetic energy, the surface and potential energy components are comparable. This approach of analysis can predict the wall wetting liquid and demarcate the domain of millichannel. The inlet composition complements the diameter effect on the stable flow pattern.

Literature Cited

1. Biswas KG, Das G, Ray S, Basu JK. Mass transfer characteristics of liquid–liquid flow in small diameter conduits. *Chem Eng Sci*. 2015; 122:652–661.
2. Kashid MN, Harshe YM, Agar DW. Liquid-liquid slug flow in a capillary: an alternative to suspended drop or film contactors. *Ind Eng Chem Res*. 2007;46:8420–8430.
3. Shinohara K, Yokoyama Y, Torii T, Okamoto K. Between microdroplets and microfluidics: unbreakable liquid/liquid interfaces at a junction of hydrophilic microchannels. *Appl Phys Lett*. 2008;93: 034103.
4. Dreyfus R, Tabeling P, Willaime H. Ordered and disordered patterns in two-phase flows in microchannels. *Phys Rev Lett*. 2003;90(14): 144505.
5. Thorsen T, Roberts RW, Arnold FH, Quake SR. Dynamic pattern formation in a vesicle-generating microfluidic device. *Phys Rev Lett*. 2001;86(18):4163–4166.
6. Dessimoz AL, Cavin L, Renken A, Minsker LK. Liquid–liquid two-phase flow patterns and mass transfer characteristics in rectangular glass microreactors. *Chem Eng Sci*. 2008;63:4035–4044.
7. Kashid M, Minsker LK. Quantitative prediction of flow patterns in liquid–liquid flow in micro-capillaries. *Chem Eng Process*. 2011;50: 972–978.
8. Jovanovic J, Zhou W, Rebrov EV, Nijhuis TA, Hessel V, Schouten JC. Liquid–liquid slug flow: hydrodynamics and pressure drop. *Chem Eng Sci*. 2011;66:42–54.
9. Zhao Y, Chen G, Yuan Q. Liquid-liquid two-phase flow patterns in a rectangular microchannel. *AIChE J*. 2006;52(12):4052–4060.
10. Tsaoulidis D, Dore V, Angeli P, Plechkova NV, Seddon KR. Flow patterns and pressure drop of ionic liquid–water two-phase flows in microchannels. *Int J Multiphase Flow*. 2013;54:1–10.
11. Ismagilov RF, Stroock AD, Kenis PJA, Whitesides G, Stone HA. Experimental and theoretical scaling laws for transverse diffusive broadening in two-phase laminar flows in microchannels. *Appl Phys Lett*. 2000;76(17):2376–2378.
12. Ahn Y, Jung W, Chen Z. Turbid two-phase slug flow in a microtube: simultaneous visualization of structure and velocity field. *Appl Phys Lett*. 2006;89:064109.
13. Chakrabarti DP, Das G, Ray S. Pressure drop in liquid-liquid two phase horizontal flow: experiment and prediction. *Chem Eng Technol*. 2005;28(9):1003–1009.
14. Brauner N, Rovinsky J, Maron DM. Determination of the interface curvature in stratified two-phase systems by energy considerations. *Int J Multiphase Flow*. 1996;22:1167–1185.
15. Brauner N. The prediction of dispersed flows boundaries in liquid-liquid and gas-liquid systems. *Int J Multiphase Flow*. 2001;27:885–910.
16. Brauner N, Ullmann A. Modeling of phase inversion phenomenon in two-phase pipe flows. *Int J Multiphase Flow*. 2002;28(7):1177–1204.
17. Sharma A, Sarkhi AA, Sarica C, Zhang HQ. Modeling of oil-water flow using energy minimization concept. *Int J Multiphase Flow*. 2011;37:326–335.
18. Dabirian R, Thompson L, Mohan RS, Shoham O, Avila C. Predication of two-phase flow splitting in looped lines based on energy minimization. In: *SPE Annual Technical Conference and Exhibition*, New Orleans, Louisiana, USA, 2013.
19. Zaghloul JS. Multiphase Analysis of Three-Phase (Gas-Condensate-Water) Flow in Pipes. Doctoral Thesis. *Pennsylvania State University, State College, Pennsylvania, 2006*.
20. Triplett KA, Ghiaasiaan SM, Abdel-Khalik SI, Sadowski DL. Gas–liquid two-phase flow in microchannels. Part I: two-phase flow patterns. *Int J Multiphase Flow*. 1999;25:377–394.
21. Mandal TK, Das G, Das PK. An appraisal of liquid–liquid slug flow in different pipe orientations. *Int J Multiphase Flow*. 2010;36:661–671.
22. Bajaras AM, Panton RL. The effects of contact angle on two-phase flow in capillary tubes. *Int J Multiphase Flow*. 1992;19(2):337–346.
23. Biswas KG, Patra R, Das G, Ray S, Basu JK. Effect of flow orientation on liquid–liquid slug flow in a capillary tube. *Chem Eng J*. 2015;262:436–446.
24. Brauner N. Modeling and Control of Two-Phase Flow Phenomena: Liquid–Liquid Two-Phase Flow Systems. Italy: CISM Center, 2002.
25. Chakraborti DP, Das G, Das PK. The transition from water continuous to oil continuous flow pattern. *AIChE J*. 2006;52(11):3668–3678.
26. Suo M, Griffith P. Two-phase flow in capillary tubes. *J Basic Eng*. 1964;86(3):576–582.

Manuscript received July 7, 2015, and revision received Aug. 22, 2015.